NOTES AND CORRESPONDENCE

Modal Bias in Sea Level and Sea Surface Temperature, with Applications to Remote Sensing

WILLIAM W. HSIEH[1]

School of Mathematics, University of New South Wales, Kensington, N.S.W., Australia, 2033

15 May 1984 and 2 November 1984

ABSTRACT

From vertical normal mode decomposition, sea level and sea surface temperature (SST) are shown to be modally biased—higher modes are suppressed in sea level while lower modes are suppressed in SST data. Having been effectively "low passed" and "high passed" (with respect to mode number) by nature, sea level and SST contain complementary information which can in principle be combined to yield a relatively unbiased picture. The full potential of the sea level–SST pair is not appreciated in present remote sensing studies, where the two are used separately. A proposed "stereoscopic" method may in the future produce unbiased three-dimensional pictures from satellite-sensed two-dimensional pictures of sea level and SST. Modal bias in coastal trapped waves is studied in the Appendix.

1. Introduction

Vertical normal mode decomposition is widely used for studying long-wave motion in a stratified, flat-bottom ocean (LeBlond and Mysak, 1978). Assuming each mode is given the same amount of potential energy, the sea level displacements are nevertheless much smaller for the higher modes, while the sea surface temperature (SST) perturbations are much weaker for the lower modes. Hence, sea level and SST data are modally biased. We can think of nature as having effectively performed a low-pass filter (with respect to mode number) on sea level data and a high-pass filter on SST data. The two types of data are thus individually incomplete yet *complementary*—and herein lies an opportunity for overcoming modal bias. Can we recombine the "high-passed" and "low-passed" information to obtain a relatively unbiased view of the ocean?

Within the foreseeable future, only SST and sea level will be available for large-scale ocean monitoring from space. Yet the full potential of the sea level–SST pair is not appreciated in present remote sensing studies, where the two are used separately. From a study of the modally biased nature of SST and sea level data (in Section 2), this note proceeds to advocate (in Section 3) that new techniques be developed to combine these two complementary data sources.

Combining two incomplete but complementary sources of information to yield a higher quality view or sound is familiar to us through three-dimensional movies and stereos. The making of a three-dimensional image (Fig. 1a) inspires Fig. 1b, where SST and sea level are combined by a "stereoscopic" method outlined in Section 3. Stereoscopic remote sensing may some day replace our present satellite pictures of SST and sea level as stereo records have replaced gramophone records.

2. Modal bias in an ocean of constant depth

We start with the inviscid, unforced linearized long-wave equations:

$$u_t - fv = -\frac{1}{\rho_0} p_x, \tag{1a}$$

$$v_t + fu = -\frac{1}{\rho_0} p_y, \tag{1b}$$

$$p_z = -\rho g, \tag{1c}$$

$$u_x + v_y + w_z = 0, \tag{1d}$$

$$\rho_t = -w\rho_{0z}, \tag{1e}$$

where u, v, w are the velocity components, p the pressure perturbation, ρ the density perturbation from the rest state $\rho_0(z)$; f the Coriolis parameter and g is the gravitational constant.

In order to perform vertical mode decomposition, we neglect topography and assume a constant depth H. Following Gill and Clarke (1974), we let

$$\begin{pmatrix} u \\ v \\ p \end{pmatrix} = \sum_n \begin{pmatrix} u_n \\ v_n \\ p_n \end{pmatrix} \hat{p}_n(z),$$

$$\begin{pmatrix} w \\ -\rho/\rho_{0z} \end{pmatrix} = \sum_n \begin{pmatrix} w_n \\ h_n \end{pmatrix} \hat{w}_n(z), \tag{2}$$

[1] Present affiliation: Department of Oceanography, University of British Columbia, Vancouver, B.C., Canada V6T 1W5.

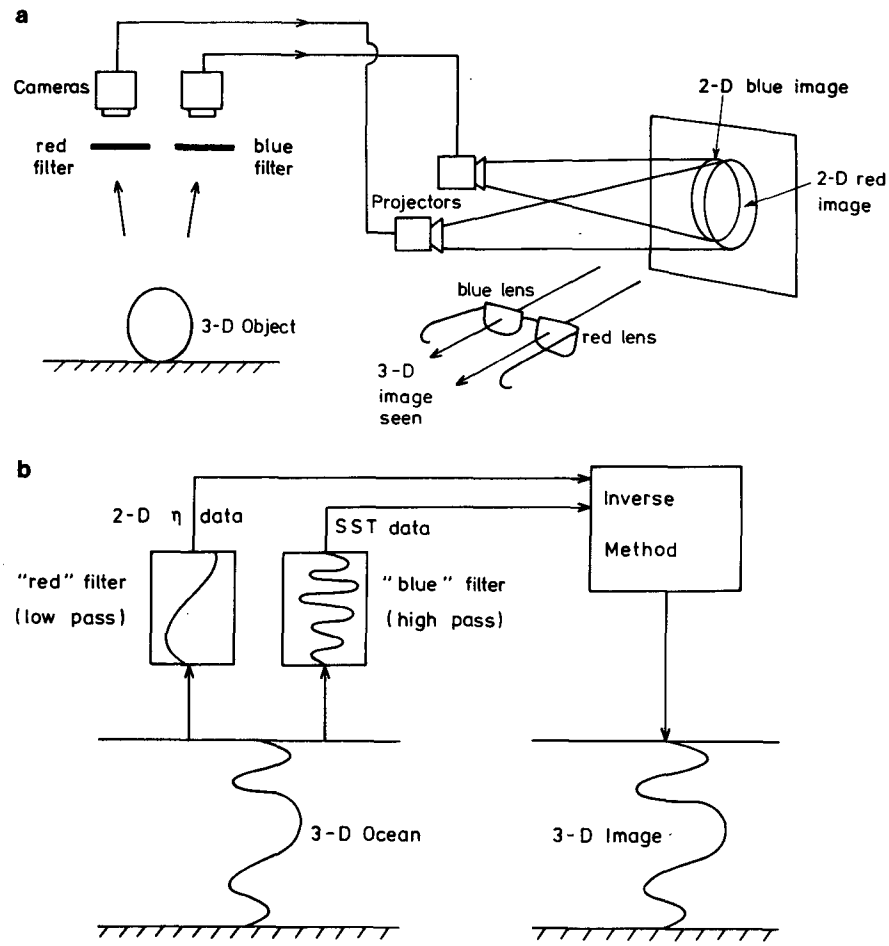

FIG. 1. (a) Creating a three-dimensional image from two two-dimensional images. The original object is photographed by two cameras spaced slightly apart, the two two-dimensional images in different colours are then projected separately, and picked up individually by each eye through coloured filters. (b) Corresponding stereoscopic method for combining SST and sea level data. Nature's bias for low modes in sea level fluctuations and for high modes in SST effectively supplies a "red" and a "blue" filter. These two filtered sources of data are then recombined by an inverse method for the least biased view.

where u_n, v_n, p_n, w_n and h_n are functions of x, y, t only, and the depth-dependent parts are marked with a circumflex. The Boussinesq approximation is assumed, where $\rho_0(z)$ in Eqs. (1a, b) is replaced by a constant ρ_*.

Separation of variables in (1d, c) gives

$$\hat{p}_n = d\hat{w}_n/dz, \tag{3a}$$

$$d\hat{p}_n/dz = -(N^2/c_n^2)\hat{w}_n, \tag{3b}$$

where c_n^2 is a constant of separation and the buoyancy frequency $N^2 = -g\rho_{0z}/\rho_*$.

a. Constant N

Assume constant N, then (3) together with the boundary conditions $\hat{w} = 0$ at $z = 0$ and $-H$ yield for the baroclinic modes,

$$\hat{p}_n = \cos(n\pi z/H), \tag{4a}$$

$$\hat{w}_n = \frac{c_n}{N}\sin(n\pi z/H), \tag{4b}$$

with $c_n = NH/(n\pi)$, $n = 1, 2, \ldots$, the internal long-wave speed for the nth mode.

From (1e), (2) and (4b), the maximum isopycnal displacement in the water column is given by

$$D_n = h_n c_n/N. \tag{5}$$

The sea surface displacement η_n is obtained from

$$p_n = \rho_* g\eta_n. \tag{6}$$

From (1c) and (3b), we obtain the ratio of the sea level displacement to the maximum isopycnal displacement for the nth mode,

$$\eta_n/D_n = Nc_n/g. \tag{7}$$

If we fix D_n (i.e., all modes having the same internal potential energy), the sea level displacement of the

modes are biased by the factor c_n, which decreases with increasing n (see also Wunsch and Gill, 1976, pp. 377–378).

For modal bias associated with SST observations, we examine the ratio of surface density perturbations ρ_s of two equally excited modes m and n (i.e., $D_m = D_n$). By (2), (4b) and (5), we have

$$\frac{\rho_{sn}}{\rho_{sm}} = \lim_{z\to 0} \frac{h_n \hat{w}_n(z)}{h_m \hat{w}_m(z)} = \lim_{z\to 0} \frac{\sin(n\pi z/H)}{\sin(m\pi z/H)} = \frac{n}{m}. \quad (8)$$

Thus, modal bias is in favor of higher modes—e.g., $\rho_{s2}/\rho_{s1} = 2$, $\rho_{sn}/\rho_{s1} = n$. Intuitively, this bias is to be expected from the vertical structure of $\sin(n\pi z/H)$, with the uppermost maximum at $z = -H/(2n)$. As n increases, this uppermost maximum moves progressively closer to the surface, thereby enhancing its influence near the surface.

b. *Realistic N(z)*

Figure 2a shows the $N(z)$ profile determined from hydrographic data off Vancouver Island by Crawford and Thomson (1984). Using this profile for $N(z)$, we integrate (3) through the water column with a flat bottom and a free surface (e.g., see LeBlond and Mysak, 1978, p. 124) to obtain the normal modes. The density perturbations $\rho(z)$ for modes 1–3 are shown in Fig. 2b.

In the absence of surface mixing, the density perturbation at the sea surface is identically zero. Recently, Stevenson (1983) investigated how baroclinic Rossby waves can be manifested in the surface temperature by connecting a Kraus-Turner (1967) surface mixed layer to the underlying quasi-geostrophic wave.

Here, we will limit ourselves to a simple model. Figure 2b shows the near-surface gradient $\partial\rho_n/\partial z$ becoming stronger with increasing mode number n. Figure 3 illustrates how the stronger gradients give rise to larger sea surface density perturbations in the presence of a mixed layer of thickness D, with

$$\rho_{sn} = \frac{1}{2} D \frac{\partial \rho_n}{\partial z}, \quad (9)$$

i.e. the surface density perturbation is directly proportional to the near-surface gradient and to the mixed layer depth.

Table 1 shows the near surface density gradients and sea level displacements for several modes and the corresponding modal bias factors $(\partial\rho_n/\partial z)/(\partial\rho_1/\partial z)$ and η_n/η_1. As vertical normal-mode decomposition is applicable to long Poincaré waves, Rossby waves, Equatorial trapped waves and coastal Kelvin waves (LeBlond and Mysak, 1978), modal bias—that higher modes are enhanced in SST but suppressed in sea level data—covers a surprisingly large class of ocean waves. In particular, for coastal Kelvin waves at a given frequency, the wavelengths are proportional to c_n, whence higher modes have shorter wavelengths.

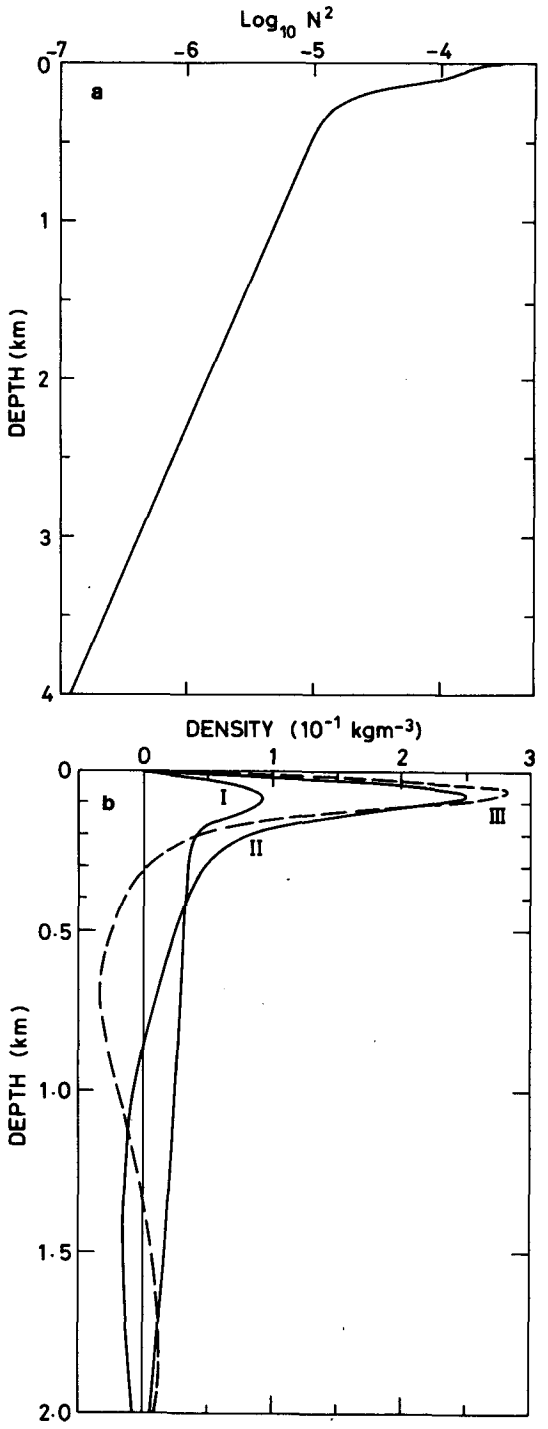

FIG. 2. (a) Buoyancy frequency $N(z)$ in s^{-1}. Ocean is 4 km deep. (b) Vertical structure of the density perturbation for modes 1, 2 and 3 (labelled I, II, III). Only the top 2 km are shown. Below 2 km, the curves taper off to zero at the bottom. The modes are normalized to have equal potential energy (10^4 kg m^2 s^{-2}) in the water column. Note the much stronger gradients $\partial\rho_n/\partial z$ near the surface for the higher modes.

Thus, alongshore length scales determined from sea level data should be considerably larger than those from SST data, as low modes dominate the sea level

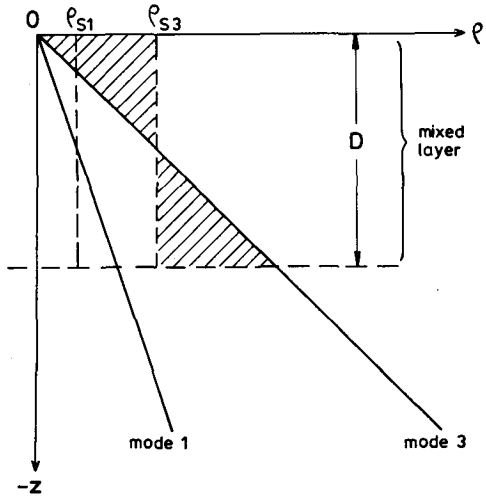

FIG. 3. Schematic diagram illustrating how the stronger gradients $\partial\rho_n/\partial z$ of the higher modes give rise to larger sea surface density perturbations ρ_{sn}. Given a surface mixed layer of depth D, kinetic energy from the wind lifts the water in the lower shaded triangle to the upper triangle, thereby producing a uniform density perturbation ρ_{s3} throughout the mixed layer for mode 3. The same mechanism gives rise to a much lower value for ρ_{s1}.

but not the SST. The effects of the continental shelf on modal bias are discussed in the Appendix.

Rhines' (1970) study of the combined effects of gently sloping topography and stratification shows that as the wavelength decreases, the waves become increasingly bottom-trapped. For higher modes with relatively shorter wavelengths, bottom-trapping would diminish the surface density gradients. Hence, surface $(\partial\rho_n/\partial z)/(\partial\rho_1/\partial z)$ values for $n > 1$ would be less than the corresponding values for a flat-bottom ocean. Furthermore, in contrast to the flat-bottom situation where $\partial\rho_1/\partial z < \partial\rho_2/\partial z < \cdots$, the presence of sloping topography would probably introduce a mode number m such that

$$\frac{\partial\rho_1}{\partial z} < \frac{\partial\rho_2}{\partial z} < \cdots < \frac{\partial\rho_m}{\partial z} > \frac{\partial\rho_{m+1}}{\partial z} > \cdots, \quad \text{at} \quad z = 0, \tag{10}$$

i.e. SST would be biased in favor of intermediate modes with mode number near m.

3. Applications to remote sensing

At a given frequency band, sea level $\eta e^{-i\omega t}$ and surface temperature $T_s e^{-i\omega t}$ can be expanded in terms of the contributions from individual modes,

$$\eta = a_0 p_0 + a_1 p_1 + a_2 p_2 + \cdots, \tag{11a}$$

$$T_s = b_0 p_0 + b_1 p_1 + b_2 p_2 + \cdots, \tag{11b}$$

where p_n is given in (2), and a_n, b_n are the modal bias factors determined from vertical normal-mode decomposition for a given stratification $N(z)$. For instance, $a_n p_n$ is the contribution to the sea level displacements by mode n, with a perturbation pressure of $p_n\hat{p}_n(z)$ in the water column [see Eq. (2)]. The quantities in (11) are complex to allow for phase lags between η, p_n and T_s.

With the series truncated after mode m, we have

$$\begin{bmatrix} a_0 & a_1 & a_2 & \cdots & a_m \\ b_0 & b_1 & b_2 & \cdots & b_m \end{bmatrix} \begin{bmatrix} p_0 \\ p_1 \\ \vdots \\ p_m \end{bmatrix} = \begin{bmatrix} \eta \\ T_s \end{bmatrix} \tag{12a}$$

or

$$\mathbf{AX} = \mathbf{Y}, \tag{12b}$$

where $\mathbf{A}$ is a complex matrix containing the modal bias factors, and $\mathbf{X}$ and $\mathbf{Y}$ are complex vectors. In reality, with the satellite data covering a horizontal grid, $\mathbf{A}$, $\mathbf{X}$ and $\mathbf{Y}$ will be much larger in size than those illustrated in (12a) where, for simplicity, the data are assumed to have come from a single location. With $\mathbf{A}$ known from normal mode decomposition and $\mathbf{Y}$ from satellite data, $\mathbf{X}$ can be determined from the inverse method (Claerbout, 1976, Wunsch, 1978). The optimal solution for $\mathbf{X}$ is given by

$$\mathbf{X} = (\mathbf{A}^H\mathbf{A})^{-1}\mathbf{A}^H\mathbf{Y} \tag{13}$$

where $\mathbf{A}^H$ is the complex conjugate-transpose of $\mathbf{A}$. With p_n known from $\mathbf{X}$, and the depth structures $\hat{p}_n(z)$ known from normal mode decomposition, we can construct the perturbation pressure field p in the water column, with

$$p = \sum_n p_n\hat{p}_n(z). \tag{14}$$

TABLE 1. Modal bias for sea surface density (temperature) and sea level perturbations, with normal modes calculated from the $N(z)$ profile shown in Fig. 2a. The modal bias factors $(\partial\rho_n/\partial z)/(\partial\rho_1/\partial z)$ and η_n/η_1 respectively show how the higher modes are stronger at sea surface density (temperature) and weaker at sea level perturbations. All modes are normalized to have the same potential energy (10^4 kg m^2 s^{-2}) in the water column. For comparison, numbers in parentheses are the corresponding values from the constant N, rigid-lid model.

	Mode n				
	0	1	2	3	10
c_n (m s^{-1})	198.	2.22	1.18	0.83	0.24
Surface $\frac{\partial\rho_n}{\partial z}$ (10^{-2} kg/m^4)	0.08	0.29	0.88	1.14	4.25
$\frac{\partial\rho_n/\partial z}{\partial\rho_1/\partial z}$ as $z \to 0$	0.28	1.0	3.0 (2.0)	3.9 (3.0)	14.5 (10.0)
Sea level η_n (cm)	140.	4.67	4.03	2.58	0.84
η_n/η_1	30. (89.)	1.0	0.86 (0.50)	0.55 (0.33)	0.18 (0.10)

We can then proceed to construct the density perturbation fields and the geostrophic velocity fields. Hence, three-dimensional pictures of the ocean are derived from the original two-dimensional sea level and SST data.

This proposed "stereoscopic" method is of course highly idealistic, and serves only to stimulate further studies. The degree of ill-posedness of such a procedure and the effects of the surface mixed layer need careful scrutiny before the feasibility of stereoscopic remote sensing can be established.

Acknowledgment. I thank Chris Garrett, Bruce Hamon, Ross Hendry and Jason Middleton for their helpful comments. I am also grateful to Ken Brink and Bill Crawford for kindly providing me with the Brink (1982) coastal-trapped wave program.

APPENDIX

Modal Bias in Coastal Trapped Waves

We let x and y be the offshore and alongshore coordinates, and assume the variables depend on y and t in the form $\exp[i(ky - \omega t)]$. At the equilibrium sea level $z = 0$,

$$p = \rho_0 g \eta, \tag{A1}$$

$$w = \eta_t = -i\omega\eta. \tag{A2}$$

The velocity component normal to the solid bottom boundary must vanish, i.e.

$$w = -u\frac{dh}{dx} \quad \text{at} \quad z = -h(x), \tag{A3}$$

where $h(x)$ is the depth. At the coast $x = 0$, $h(0) = 0$. Let $dh/dx = \alpha$ at $x = 0$; (A2) and (A3) at $x = 0$ give

$$U = \frac{i\omega}{\alpha}\eta_c, \tag{A4}$$

where U and η_c are the values of u and η at the coast. Substituting (A1) and (A4) into (1b) at $x = 0$ gives

$$V = \left(\frac{g}{c} + \frac{f}{\alpha}\right)\eta_c, \tag{A5}$$

where $c = \omega/k$ and V, the value of v at the coast. Equations (A4) and (A5) relate the horizontal current components U, V to the coastal sea level η_c at the coast. Analogous relations have been used by Battisti and Clarke (1982a,b) to predict the barotropic tidal currents from the coastal sea level. As we have started with Eqs. (1), the three-dimensional equations for a stratified fluid, instead of the two-dimensional barotropic equations as in Battisti and Clarke, the derivation here is in some sense a generalization of the Battisti and Clarke result to a stratified ocean and coastal trapped waves.

For monotonically increasing depth $h(x)$, Huthnance [1978, Eq. (2.7)] proves that for any given $k > 0$, an infinite number of modes exists with $|\omega_0| > |\omega_1| > |\omega_2| > \cdots$ (or $|c_0| > |c_1| > \cdots$), where in our coordinate system, the ω_n and c_n are negative in the Northern Hemisphere. Thus the two terms within the parentheses in (A5) have opposite signs, and depending on whether their sum is positive or negative, V and η_c are respectively in-phase or 180° out-of-phase.

For typical continental shelves, the slope $\alpha \sim 10^{-3}$, giving $|g\alpha/f| \sim 10^2 \text{m s}^{-1}$ at midlatitudes. As this is a relatively large value, only the $n = 0$ mode (corresponding to the barotropic Kelvin wave modified by the continental shelf) is likely to satisfy $|c_0| > |g\alpha/f|$ ($|c_0| \approx \sqrt{gH} = 200$ m s^{-1} for $H = 4$ km). All other modes ($n \geq 1$) tend to satisfy $|c_n| \ll |g\alpha/f|$, so

$$\frac{\eta_c}{V} = \left(\frac{g}{c_n} + \frac{f}{\alpha}\right)^{-1} \approx \frac{c_n}{g} \tag{A6}$$

to a very good approximation; i.e., in contrast to the $n = 0$ mode, the higher modes are not significantly affected by the coastal slope α. For a given V, η_c is directly proportional to c_n, i.e., *the faster the mode propagates, the larger the relative sea level displacements.* For these subinertial modes, the kinetic energy of the horizontal currents is very much larger than the potential energy associated with the sea level displacements. At a particular frequency, the coastal alongshore velocity V is a sum of contributions from all possible modes, i.e. $V = V_0 + V_1 + V_2 + \cdots$. The coastal sea level is, however, weighted or biased as follows

$$\eta_c = b_0 V_0 + b_1 V_1 + b_2 V_2 + \cdots, \tag{A7}$$

where the "bias factors" $b_n \equiv \eta_{cn}/V_n$ are given by (A6). Since $|c_0| > |c_1| > |c_2| > \cdots$ from Huthnance (1978), (A6) yields $|b_0| > |b_1| > |b_2| > \cdots$. Hence we conclude that for subinertial motion, the sea level data are biased in favour of the low modes, which propagate faster. Consequently, alongshore phase speeds estimated from sea level data are almost invariably higher than corresponding estimates from current data, with examples given in Hsieh (1982).

The relations (A4) and (A5) between coastal currents and sea level are surprisingly general. They are also valid for suprainertial frequencies, $|\omega| > |f|$, i.e., *edge waves.* However, in contrast to the subinertial modes, Huthnance (1975) proved that $|c_0| < |c_1| < |c_2| < \cdots$ for the edge waves, so η_c/V is biased in favor of the *high* modes. Furthermore, if $h(x)$ is not monotonically increasing, e.g., in the presence of trenches or banks off the coast, additional trapped modes may be present (Mysak *et al.*, 1979; Brink 1983; Middleton, 1983). Equations (A4) and (A5) still govern the coastal behavior of these extra modes.

Frictional effects which are important in shallow water may however modify these relations (Battisti and Clarke, 1982a, p. 9). For a viscous fluid, even the alongshore velocity must vanish at the shore. Thus V in (A5) must be interpreted as the alongshore velocity just outside the coastal viscous boundary layer.

Finally, a cautionary note on the use of shelf models with a small coastal wall. With $u = 0$ at the coast, the term f/α disappears from (A6) and $\eta_c/V = c_n/g$. While this is accurate for the $n \geq 1$ subinertial modes it is incorrect for the Kelvin mode (and the edge wave modes). For instance, for a typical shelf with $\alpha = 1.5 \times 10^{-3}$, $f = 10^{-4}$ s^{-1}, $c_0 = -200$ m s^{-1}, then $g/c_0 = -0.05$ s^{-1}, while $f/\alpha = +0.067$ s^{-1}. The exact relation (A5) gives $\eta_c/V = +60$ s, whereas models with a small coastal wall predict $\eta_c/V = c_0/g = -20$ s. Thus, not only is the sea level too small by a factor of 3, but η_c and V are out-of-phase instead of in-phase! Many researchers using such models for barotropic Kelvin waves (or edge waves) seem unaware that the small coastal wall leads to incorrect coastal sea level values despite having correct shelf topography in their models.

The SST modal bias in coastal waters is more difficult to quantify. Without a continental shelf, the modes trapped against the vertical wall in a flat-bottom ocean are the surface and internal Kelvin waves, which are biased in SST in favor of the higher modes (Table 1). With a continental shelf, the modes $n \geq 1$ resemble internal Kelvin waves only at low latitudes, but become quasi-barotropic shelf waves at higher latitudes (Brink, 1982). Using Brink's coastal trapped wave program and the $N(z)$ of Fig. 2a, we computed the modal structures for a "typical" continental shelf (with a coastal wall of 1 m, a linear slope of 1:400 from coast to shelf break at the 150 m isobath, and a smooth joint to a continental slope of gradient ~ 0.1). At 10°N, with the same energy in modes 1 and 2, the surface modal bias $(\partial\rho_2/\partial z)/(\partial\rho_1/\partial z)$ values are 2.7, 1.8 and 1.1 respectively at 0, 40 and 80 km offshore (i.e., at the 1, 100 and 1000 m isobaths), which are smaller than those from the flat-bottom model. The offshore decrease in the modal bias is due to the faster offshore decay of mode 2 relative to mode 1. As we moved to higher latitudes, surface $\partial\rho/\partial z$ values from Brink's model diminish, (e.g., surface $\partial\rho/\partial z$ values for modes 1 and 2 at 50° are only about half as large as those at 10°).

In summary, for coastal trapped waves, modal bias in sea level data, as suggested by Hsieh (1982), has been quantified by (A6). For SST, Brink's (1982) program shows the second mode to be enhanced with respect to the first mode. However, the importance of modal bias in the coastal SST is less clear since the waves become quasibarotropic at mid to high latitudes, and much of coastal SST variability is caused by river runoff, fronts, local upwelling, etc.

REFERENCES

Battisti, D. S., and A. J. Clarke, 1982a: A simple method for estimating barotropic tidal currents on continental margins with specific application to the M_2 tide off the Atlantic and Pacific coasts of the United States. *J. Phys. Oceanogr.*, **12**, 8–16.

——, and ——, 1982b: Estimation of nearshore tidal currents on nonsmooth continental shelves. *J. Geophys. Res.*, **87**, 7873–7878.

Brink, K. H., 1982: A comparison of long coastal-trapped wave theory with observations off Peru. *J. Phys. Oceanogr.*, **12**, 897–913.

——, 1983: Low-frequency free wave and wind-driven motions over a submarine bank. *J. Phys. Oceanogr.*, **13**, 103–116.

Claerbout, J. F., 1976: *Fundamentals of Geophysical Data Processing*, McGraw-Hill, 274 pp.

Crawford, W. R., and R. E. Thomson, 1984: Diurnal period continental shelf waves along Vancouver Island: A comparison of observations and numerical models. Submitted to *J. Phys. Oceanogr.*

Gill, A. E., and A. J. Clarke, 1974: Wind-induced upwelling, coastal currents and sea-level changes. *Deep Sea Res.*, **21**, 325–345.

Hsieh, W. W., 1982: On the detection of continental shelf waves. *J. Phys. Oceanogr.*, **12**, 414–427.

Huthnance, J. M., 1975: On trapped waves over a continental shelf. *J. Fluid Mech.*, **69**, 689–704.

——, 1978: On coastal trapped waves: Analysis and numerical calculation by inverse iteration. *J. Phys. Oceanogr.*, **8**, 74–92.

Kraus, E. B., and J. S. Turner, 1967: A one-dimensional model of the seasonal thermocline, II. The general theory and its consequences. *Tellus*, **19**, 98–106.

LeBlond, P. H., and L. A. Mysak, 1978: *Waves in the Ocean.* Elsevier, 602 pp.

Middleton, J. H., 1983: Low-frequency trapped waves on a wide, reef-fringed continental shelf. *J. Phys. Oceanogr.*, **13**, 1371–1382.

Mysak, L. A., P. H. LeBlond and W. J. Emery, 1979: Trench waves. *J. Phys. Oceanogr.*, **9**, 1001–1013.

Rhines, P. B., 1970: Edge-, bottom-, and Rossby waves in a rotating stratified fluid. *Geophys. Fluid Dyn.*, **1**, 273–302.

Stevenson, J. W., 1983: The seasonal variation of the surface mixed-layer response to the vertical motions of linear Rossby waves. *J. Phys. Oceanogr.*, **13**, 1255–1268.

Wunsch, C., 1978: The North Atlantic general circulation west of 50°W determined by inverse methods. *Rev. Geophys. Space Phys.*, **16**, 583–620.

——, and A. E. Gill, 1976: Observations of equatorial trapped waves in Pacific sea-level variations. *Deep Sea Res.*, **23**, 371–390.